

RSC Advances



This is an *Accepted Manuscript*, which has been through the Royal Society of Chemistry peer review process and has been accepted for publication.

Accepted Manuscripts are published online shortly after acceptance, before technical editing, formatting and proof reading. Using this free service, authors can make their results available to the community, in citable form, before we publish the edited article. This *Accepted Manuscript* will be replaced by the edited, formatted and paginated article as soon as this is available.

You can find more information about *Accepted Manuscripts* in the [Information for Authors](#).

Please note that technical editing may introduce minor changes to the text and/or graphics, which may alter content. The journal's standard [Terms & Conditions](#) and the [Ethical guidelines](#) still apply. In no event shall the Royal Society of Chemistry be held responsible for any errors or omissions in this *Accepted Manuscript* or any consequences arising from the use of any information it contains.



Journal Name

ARTICLE

Harmonization of upconverting nanocrystals and photosensitizer for antimicrobial application†

Received 00th January 20xx,
Accepted 00th January 20xx

DOI: 10.1039/x0xx00000x

www.rsc.org/

Thapakorn Tree-Udom,^a Patchanita Thamyongkit,^b Nawaporn Wiratkasem,^c Chanpen Chanchao,^d Tanapat Palaga,^e Numpon Insin,^b, Sirirat Rengpipat,^e and Supason Wanichwecharungruang^{*b,f}

Although the loading of photosensitizers onto upconverting nanoparticles (UCs) has been demonstrated previously, none of the works has perfected the matching between absorption wavelengths of the loaded photosensitizers and emission wavelengths from UCs. Therefore not all visible emissions from UCs are used purposefully. In addition, low upconversion of near infrared radiations into UV-visible emissions by the UCs has hindered applications of the materials. Here we show that by optimizing the doping amount of Tm³⁺ in the Yb³⁺-doped NaYF₄ lattice and constructing a NaYF₄ shell around the optimized [Yb³⁺, Tm³⁺-doped NaYF₄ core], UVA and visible emissions can be tremendously increased. We also synthesize *meso*-tetraphenyltetrabenzoporphyrinatozinc (ZnTPTBP), a photosensitizer whose absorption wavelengths match perfectly with the visible emission wavelengths of the obtained UCs. We then load the ZnTPTBP onto the optimized UCs and verify an ability of the ZnTPTBP-loaded UCs to effectively generate excited singlet oxygen species upon NIR irradiation using 9,10-anthracenediyl-bis(methylene)dimalonic acid as a singlet oxygen fluorescence probe, and sodium azide as a singlet oxygen scavenger. Effective eradication of *Propionibacterium acnes* (*P. acnes*) by a combination of ZnTPTBP-loaded UCs and 980 nm laser is verified in vitro. This anti-*P. acnes* application demonstrates the total utilization of both UVA and visible emissions from the UCs; the direct excitation of *P. acnes* porphyrins by UVA emission, and the excitation of the loaded ZnTPTBP by the visible emissions which results in the production of reactive oxygen species that harm the bacteria. This work not only demonstrates an antibacterial application of UCs with high UV-visible upconverted emissions, but also shows the perfect tailoring of the materials based on the harmony between upconversion emissions and photosensitizer absorptions.

Introduction

Photodynamic therapy (PDT) has been well clinically accepted as a minimally invasive treatment for several diseases.^{1,2} In PDT, light is used to activate photosensitizer molecules from their ground state into an excited state, and the excited photosensitizers then transfer the absorbed energy to oxygen molecules to generate reactive oxygen species which are used for various purposes such as killing cancer cells and degrading tissues. At present, most

photosensitizers are excited by visible light, thus limiting their effectiveness when the target is not at the surface. This is because the biological tissues are not transparent for visible light. Biological tissues usually possess minimum light absorption in the range of 700-1000 nm or the near infrared (NIR) region, however, most photosensitizers cannot be excited by NIR light.

Upconverting nanoparticles or UCs are luminescent materials that can absorb at least two low-energy photons and radiate higher-energy photons. When the UCs are excited by NIR light, they can emit ultraviolet (UV), visible (Vis) and NIR radiations.³ As mentioned above that normal biological systems are NIR transparent (700-1000 nm), bio-imaging with UCs is not only interference free but also possible at deep locations with minimal harm to surrounding biological components and tissues.⁴⁻⁶ High photostability of the UCs even after being continuously excited by NIR are other advantages of the materials.⁷⁻⁸ UCs have been applied for multimodal imaging,⁹⁻¹¹ gene and drug delivery,¹¹⁻¹⁴ and PDT.¹⁵⁻¹⁹ Nevertheless, upconversion of photons by UCs is the improbable electronic transition process, therefore, utilization of UCs still faces a problem of low upconversion. As a result, fabricating UCs with more upconversion efficiency is needed. In addition, designing the

^a Nanoscience and Technology program, Graduate School, Chulalongkorn University, Thailand.

^b Department of Chemistry, Faculty of Science, Chulalongkorn University, Thailand.

^c Program in Biotechnology, Faculty of Science, Chulalongkorn University, Thailand.

^d Department of Biology, Faculty of Science, Chulalongkorn University, Thailand.

^e Department of Microbiology, Faculty of Science, Chulalongkorn University, Thailand.

^f Nanotec-CU Center of Excellence on Food and Agriculture, Thailand. E-mail: psupason@chula.ac.th

†Electronic Supplementary Information (ESI) available: Detailed experimental methods including materials, instruments, synthesis and characterization of core-UCs, core/shell UCs, PEO-UCs and ZnTPTBP, and cytotoxicity test of the materials. Table S1 and Figures S1-S8. See DOI: 10.1039/x0xx00000x

system that all UV and visible emissions from UCs are to be used purposefully should be beneficial.

Propionibacterium acnes (*P. acnes*) is a porphyrin-producing, oxygen tolerant, anaerobic bacterium mostly located in pilosebaceous follicles of human skin. Its porphyrins, coproporphyrin III (CPIII) with a small proportion of protoporphyrin IX (PpIX), normally absorb UVA (320 or 360 nm) and visible (407-420 nm) lights.²⁰ When *P. acnes* are exposed to blue light (407-420 nm), the porphyrins are activated and photodynamic reactions then take place, resulting in the destruction of *P. acnes*. A previous *in vitro* study has shown that irradiation of *P. acnes* with blue light alone can cause photo-excitation of the endogenous bacterial CPIII which leads to singlet oxygen production and subsequently bacterial destruction.²¹ An addition of 5-aminolaevulinic acid, a porphyrin precursor, into *P. acnes* culture, can cause an overproduction of endogenous porphyrin in *P. acnes*, resulting in a more effective photodynamic destruction of the bacteria upon the blue light irradiation.²²

Since we have noticed that the UVA emissions from Yb³⁺, Tm³⁺-doped NaYF₄ UCs are at the same wavelengths as the UVA absorption wavelengths (320-360 nm) of *P. acnes*, we speculate that the combination of this UCs and NIR may be harmful to *P. acnes*. Nevertheless, UVA emission intensity of the Yb³⁺, Tm³⁺-doped NaYF₄ is normally low. If this UCs is to be used for anti-acne application, its UVA emission intensity must be increased. In this paper, we, therefore, optimize the doping amount of the Tm³⁺ in the Yb³⁺-doped NaYF₄ lattice and construct NaYF₄ shell around the optimized [Yb³⁺, Tm³⁺-doped NaYF₄ core], in order to maximize an ability of the material to upconvert NIR into UVA and visible emissions.

In addition to a direct attack of *P. acnes* with UVA emissions from UCs upon NIR irradiation, here we load of photosensitizers onto the UCs so that the particles' visible emissions can excite the loaded photosensitizers and the excited photosensitizers can then produce reactive oxygen species to additionally harm *P. acnes*. Although the loading of photosensitizers onto UCs has been demonstrated previously for several anti-tumor applications,¹⁶⁻¹⁹ none of the works has perfected the matching between absorption wavelengths of the photosensitizer and the visible emission wavelengths from UCs. Therefore, in this work, besides fabricating UCs with maximum UVA emissions for the direct *P. acnes* attack, we synthesize a photosensitizer whose absorption wavelengths match perfectly with the visible emission wavelengths of our optimized UCs. In other words, we not only maximize the UV and visible emissions of the UCs, but also show the system that can use all the UV and visible emissions for the anti-*P. acnes* application. Finally, we preliminarily evaluate cytotoxicity of the system in human cancer skin (A-375) cell line, and proof the anti-*P. acnes* of the system *in vitro*.

Experimental

Materials and Methods

Details of materials and instruments used in the experiments are shown in S1 and S2 of the electronic supporting information (ESI).

Synthesis of upconverting nanocrystals (UCs)

Detailed synthesis procedure is shown in S3 of the ESI. The upconverting nanocrystal used in *P. acnes* eradication experiment

was a core/shell UC coated with poly(ethylene oxide) diacid (COOH-PEO-COOH) ligands, synthesized by first preparing the core UC and then growing shell around the obtained UC core, and finally coating the COOH-PEO-COOH ligands around the obtained core/shell UC. The 30 mol % Yb³⁺ doped NaYF₄ with various co-doping amounts of Tm³⁺ were first synthesized. The obtained (30 mol% Yb³⁺ and 0.2 mol% Tm³⁺)-doped NaYF₄ crystal, which possesses maximum emission in the UV-visible region (see details in result section), was used as a core crystal. Core/shell UCs was then synthesized by growing NaYF₄ around the core crystal. Finally, the COOH-PEO-COOH ligands were put around the [(30 mol % Yb³⁺ and 0.2 mol % Tm³⁺)-doped NaYF₄]/NaYF₄ core/shell nanocrystal to produce (COOH-PEO-COOH)-coated-[(30 mol% Yb³⁺ and 0.2 mol% Tm³⁺)-doped NaYF₄]/NaYF₄] or the so-called PEO-UC. The product was characterized by X-ray diffraction (XRD), inductive coupled plasma optical emission spectrometry (ICP-OES), transmission electron microscopy (TEM), attenuated total reflectance fourier transform infrared spectroscopy (ATR-FTIR) and dynamic light scattering (DLS) (see details in S4 of the ESI).

Upconversion luminescence spectroscopy

Upconverted emission spectra were obtained under excitation with a 980 nm continuous-wave laser coupled to 1 m optical fiber (Changchun New Industries Optoelectronics Technology, Changchun, China). The upconverting nanocrystals were dispersed in hexane or milliQ water and placed in a QS quartz cuvette (path length of 1 cm). The upconverted emissions were detected at 90 ° with respect to the laser excitation beam using a USB2000 fiber optic spectrometer (Ocean Optics, FL, USA).

Synthesis of meso-tetraphenyltetrabenzoporphyrinatozinc (ZnTPTBP)

ZnTPTBP was prepared according to the previously described methodology (see S5 in the ESI for synthesis details).^{23,24} In short, the 5,10,15,20-tetraphenyltetrahydro-tetrabenzoporphyrins was first synthesized and then further reacted with dichloro-5,6-dicyano-1,4-benzoquinone to obtain 5,10,15,20-tetraphenyltetrabenzoporphyrins (H₂TPTBP). After that, the zinc metallation of H₂TPTBP was performed using Zn(OAc)₂·2H₂O as a reagent. The obtained ZnTPTBP was purified by column chromatography.

ZnTPTBP: green powder, >95% purity determined by ¹H-NMR spectroscopy. ¹H-NMR (D₂O, 400 MHz): δ 7.17 (dd, 8H, *J* = 6.0, 3.2 Hz), 7.29 (dd, 8H, *J* = 6.0, 3.2 Hz), 7.87 (t, 8H, *J* = 7.2 Hz), 7.95 (t, 4H, *J* = 7.2 Hz), 8.31 (d, 8H, *J* = 7.2 Hz); MALDI-TOF-MS *m/z* obsd 875.598 [M⁺], calcd 876.223 [M = C₆₀H₃₆N₄Zn]; λ_{abs} (ε, toluene) 470 (1.9×10⁵), 613, 656 nm; λ_{abs} (3% aqueous DMSO) 465, 612, 655 nm; λ_{em} (λ_{ex} = 470 nm, toluene) 666, 731 nm.

Loading of ZnTPTBP onto PEO-UCs

Solution of ZnTPTBP in dimethyl sulfoxide (DMSO) (1000 ppm, 30 μL) was added into an aqueous suspension (1.0 mL) containing PEO-UCs (1 mg). The mixed solution was vortexed for 30 min at room temperature to allow the adsorption of ZnTPTBP onto the PEO-UCs.

To evaluate the amount of unloaded ZnTPTBP, the suspension was centrifuged and the free ZnTPTBP in the supernatant was determined using an Optizen Pop QX UV-Vis spectrophotometer (Mecasys, Daejeon, Republic of Korea) with the aid of a calibration curve. The loading content of ZnTPTBP on the UCs could then be obtained by subtracting the unloaded amount from the amount used originally. Direct quantitation of Zn in the obtained ZnTPTBP-UCs by an ICP-OES spectrometer (Optima 7000DV Perkin Elmer, MA, USA) was also carried out. Cytotoxicity of the obtained ZnTPTBP-loaded UCs was determined in human cancer skin cell line (A-375) under NIR and no NIR irradiation conditions as described in S6 of the ESI.

Measurement of singlet oxygen production

Sample (PEO-UCs or ZnTPTBP-UCs, 0.5 mg) was dispersed in 1.0 mL of milliQ water containing 10 μ M of 9,10-anthracenediyl-bis(methylene)dimalonic acid (ABDA) dye. The as-prepared mixture was placed in 1.0 mL quartz cuvette and then irradiated with a 980 nm laser at 8.0 W/cm² from time 0 to 70 seconds which corresponded to the laser exposure of 0 to 560 J/cm². The fluorescence emission of the mixture ($\lambda_{\text{ex}} = 380$ nm and $\lambda_{\text{em}} = 430$ nm) was then measured using a Cary Eclipse fluorescence spectrophotometer (Agilent Technologies, CA, USA). Similar experiment was carried out with an addition of sodium azide (10 mM).

In vitro antimicrobial photodynamic action

P. acnes (DMST 14916, purchased from the Department of Medical Sciences, Thailand) was incubated in brain heart infusion (BHI) broth (Difco, NJ, USA) at 37 °C for 72 h under anaerobic conditions using the bioMérieux GasPak and the bioMérieux Generbox anaer systems (bioMérieux, Marcy l'Etoile, France). The absorbance at 600 nm was measured by a microplate reader to estimate bacterial growth, and bacterial suspension was then adjusted to yield approximately 1.5×10^8 colony-forming units (CFU)/mL with fresh medium. The experiment was tested in sterile 96-well plates. Fifty μ L of sample (PEO-UCs, ZnTPTBP and ZnTPTBP-UCs) was added to each well containing 50 μ L of the bacterial suspension in BHI broth. Control well contained only bacterial suspension (water was added in place of sample). Negative control well contained only bacterial medium. Triplicate wells were performed for each tested condition. After incubation at 37 °C under anaerobic conditions for 4 h, the wells were irradiated with a 980 nm laser. The laser was vertically placed above the well plate with the laser power adjusted to 8.0 W/cm². Irradiation times of 0, 30, 40, 50 and 60 seconds were used and these corresponded to the laser exposures of 0, 240, 320, 400 and 480 J/cm², respectively. Then, the well plates were reincubated at the same condition until the complete 72 h. To determine the growth of *P. acnes*, 5 μ L of p-iodonitrotetrazolium violet (INT) (4 mg/mL) were added to each well, and a color change was monitored. The minimum inhibitory concentration (MIC) was defined as the lowest concentration of a test sample that inhibited the *P. acnes* growth, as indicated by the no color change after addition of INT. To evaluate the minimum bactericidal

concentration (MBC), a loopful of bacterial suspension from each well was plated on BHI agar. The agar plates were incubated at 37 °C for 72 h under anaerobic conditions, and then colonies of *P. acnes* were counted. The MBC was defined as the lowest concentration of a test sample that prevented the *P. acnes* growth, as indicated by the lack of bacterial colonies after subculture onto a BHI agar plate. MIC and MBC values were determined using the laser power of 8.0 W/cm² with the exposure time of 70 seconds and this corresponded to the laser exposure of 560 J/cm². Two independent experiments were performed with triplicate samples.

Results and discussion

Synthesis and characteristics of UCs

The 30 mol % Yb³⁺-doped NaYF₄ co-doped with 0.2, 0.5, 1.0 and 1.5 mol % Tm³⁺ upconverting nanocrystals were successfully synthesized by a thermal decomposition method in the presence of oleic acid and octadecene. The contents of Y³⁺, Yb³⁺ and Tm³⁺ in the products were analyzed by ICP-OES technique and the results (Table S1 in the ESI) revealed that the concentrations of the trivalent cations in the obtained nanocrystals agreed well with the original molar ratios of the added precursors.

All four products with different Tm³⁺ doping contents possessed hexagonal phase structure as confirmed by their XRD patterns (referenced to the standard pattern of β -NaYF₄, JCPDS file No. 28-1192) (Figure 1 and Figure S1 in the ESI).

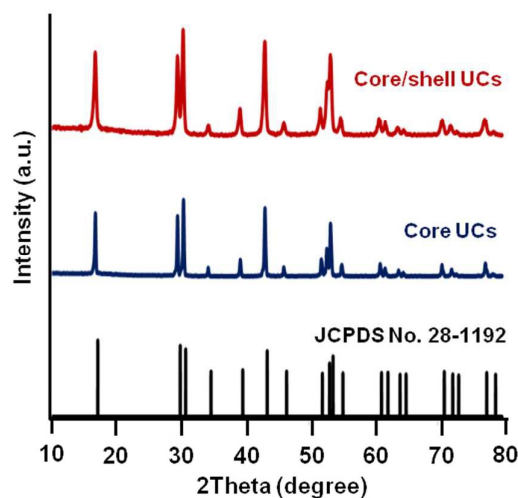


Figure 1. XRD patterns of (30 mol % Yb³⁺, 0.2 mol % Tm³⁺)-doped NaYF₄ core UCs and [(30 mol % Yb³⁺, 0.2 mol % Tm³⁺)-doped NaYF₄]/NaYF₄ core/shell-UCs.

Upon the 980 nm diode laser excitation, all the 30 mol % Yb³⁺-doped β -NaYF₄ with different Tm³⁺ co-doping contents (0.2, 0.5, 1.0 and 1.5 mol %) gave emission peaks at 290, 350, 365, 450, 475, 635 and 800 nm, and these emissions agree well with previous reports.^{25,26} However, it was observed that the intensities of peaks in the UV and visible regions increased with the decreased Tm³⁺ content in the nanocrystals. The crystals with 0.2 mol % Tm³⁺

doping content gave the highest UV-visible emission intensities (approximately 2, 10 and 100 times over those with 0.5, 1.0 and 1.5 mol % of Tm^{3+} as estimated from integration of peak area in the emission spectra, Figure 2a). We explain this observation by a concentration quenching effect in which the increase of Tm^{3+} concentration results in a decrease of the distance between adjacent Tm^{3+} dopant ions in the lattice, leading to the increase of the cross-relaxation that then reduces the radiative relaxation and thus suppresses the upconversion emission. In addition, higher numbers of Tm^{3+} in the lattice results in lower numbers of excitation photons available for each Tm^{3+} .²⁷

The obtained (30 mol % Yb^{3+} , 0.2 mol % Tm^{3+})-doped $\beta\text{-NaYF}_4$, which gave the highest upconverted UV-visible emission, was selected as a core particle for further construction of core/shell upconverting nanocrystals. We constructed the core/shell UCs by growing NaYF_4 around the (30 mol % Yb^{3+} , 0.2 mol % Tm^{3+})-doped $\beta\text{-NaYF}_4$ nanocrystalline nuclei (see Figure 2b for the models of core UCs and core/shell UCs). The XRD pattern of the obtained [(30 mol % Yb^{3+} , 0.2 mol % Tm^{3+})-doped $\beta\text{-NaYF}_4$]/ NaYF_4 core/shell nanocrystals (denoted as core/shell UCs) agreed well with the standard pattern of $\beta\text{-NaYF}_4$ (JCPDS file No. 28-1192) (Figure 1), confirming that these core/shell nanocrystals remained in a pure hexagonal phase. At a similar mass to volume concentration, under the 980 nm excitation, the upconversion emission intensity of the core/shell UCs was obviously higher than that of the core UCs (Figure 2c). To estimate the change in upconversion efficiency after the shell construction, emissions of the core-UCs and the core/shell-UCs were compared. The upconversion efficiency of the core/shell UCs was approximately 5 times of that of the core UCs (Figure 2c and Table S2 in ESI). This scenario was previously reported in another UC system by Yi and co-workers, and the authors explained an increase in upconversion efficiency upon a shell construction through the protection of energy dissipating from the core by the shell.²⁸

To make the core/shell UCs dispersible in water so they could be used in biological systems, original oleate ligands were replaced by COOH-PEO-COOH (mw = 600) via a ligand exchange strategy. Successful exchange was verified through the disappearance of the absorption peaks at 2921 and 2852 cm^{-1} (C-H stretching of the hydrocarbon chain of oleic acid) and the appearance of absorption peak at 1105 cm^{-1} (C-O-C stretching of the polyethylene oxide) in the ATR-FTIR spectrum of the product (Figure S2 in the ESI). The interaction between the PEO-diacid ligand and the UCs was likely the binding of the carboxylate functionality to the surface of the nanocrystal (Figure 2b). Large asymmetrical stretching peak of carboxylate functionality (1594 cm^{-1}) in the FTIR spectrum of the PEO-UCs (Figure S2 in the ESI) also supported our speculation. Theoretically, the binding of carboxylate to the nanocrystal surface should fix the orientation of the carboxylate moieties to a specific asymmetrical orientation, thus increasing the asymmetrical vibrational mode of this functional group. This carboxylate-nanocrystal surface interaction was also observed in the FTIR spectrum of the oleate-coated core/shell UCs (Figure S2 in ESI). Another evidence for the successful ligand exchange was the good

water dispersibility of the PEO-UCs product with the zeta potential of -25.9 ± 2.97 mV. It should be noted here that the ligand exchange did not alter the optical property of the nanocrystals, i.e., the emission spectrum of PEO-UCs was the same as that of the oleate-coated core/shell UCs (Figure 2c, Table S2).

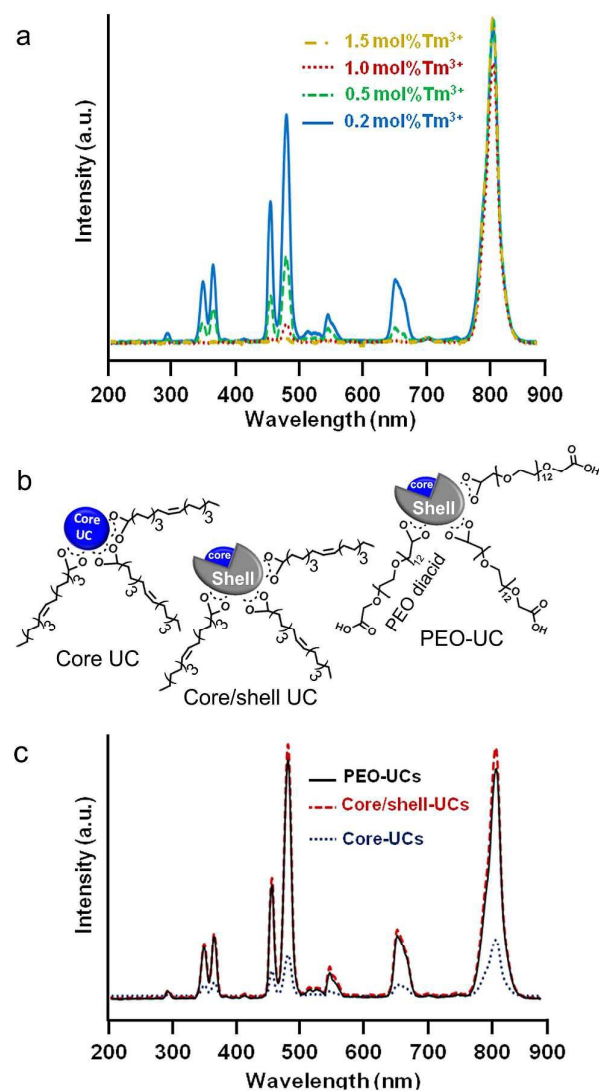


Figure 2. Different upconverting nanoparticles and their emission spectra: a) Emission spectra of core-UCs of different mol % of Tm^{3+} in hexane; b) Models of core UCs, core/shell-UCs (the material before ligand exchange) and PEO-UCs (the material after ligand exchange); and c) Emission spectra of (30 mol % Yb^{3+} , 0.2 mol % Tm^{3+})-doped NaYF_4 -core-UCs in hexane, [(30 mol % Yb^{3+} , 0.2 mol % Tm^{3+})-doped NaYF_4]/ NaYF_4 core/shell-UCs in water, and (COOH-PEO-COOH)-coated [(30 mol % Yb^{3+} , 0.2 mol % Tm^{3+})-doped NaYF_4]/ NaYF_4 core/shell-UCs or PEO-UCs in water. In a and c, concentration of the material was 1000 $\mu\text{g}/\text{mL}$, and $\lambda_{\text{ex}} = 980$ nm.

Transmission electron microscopic analysis of the core UCs, the core/shell UCs, and the PEO-UCs revealed similar elongated spherical morphology (Figure 3), however, significant increase in

size upon the shell construction was observed, i.e., the core alone showed elongated spherical shape with an average length/width of $17.49 \pm 2.10/14.96 \pm 1.85$ nm (aspect ratio ~ 1.2) whereas average length/width of the core/shell UCs was $30.74 \pm 1.22/23.36 \pm 0.75$ nm (aspect ratio ~ 1.3) (Figure 3a and 3b). Exchange of oleate ligands into COOH-PEO-COOH ligands neither significantly affected the size nor the morphology of the particles, i.e., average length/width of $31.78 \pm 1.20/24.72 \pm 1.25$ nm with aspect ratio of ~ 1.3 was observed for the PEO-UCs (Figure 3b and 3c). In summary, we have successfully synthesized water dispersible nanocrystals of (COOH-PEO-COOH)-coated $[(30 \text{ mol } \% \text{ Yb}^{3+}, 0.2 \text{ mol } \% \text{ Tm}^{3+})\text{-doped NaYF}_4]/\text{NaYF}_4$ core/shell-UCs or PEO-UCs with high upconverted emission in the UV-visible regions.

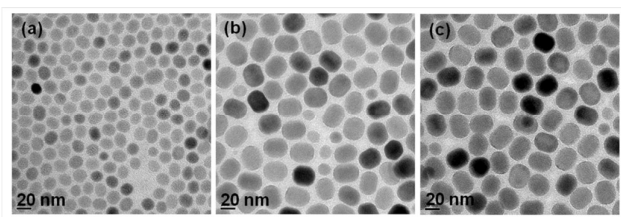


Figure 3. Representative TEM images of (a) core-UCs, (b) core/shell-UCs and (c) PEO-UCs.

Synthesis of ZnTPTBP

Porphyrins are highly conjugated macrocycle organic compounds with strong absorption of visible light. These molecules are involved in a number of biological roles, including oxygen transport (heme in red blood cell) and photosynthesis (chlorophyll in leaf). Various porphyrins have been used as fluorescence imaging, photodynamic therapeutic and theranostic agents.²⁹ Complex of metal and porphyrin has also been used as an oxidizing agent.^{30,31} Absorption wavelength of porphyrins can be tuned by modifying their chemical structures.³² Here we tuned the chemical structure of porphyrin to finally obtain *meso*-tetraphenyltetraabenzoporphyrinatozinc (ZnTPTBP) with strong absorption at 430-490 nm and weak absorption at 630 nm. Its absorption bands, indeed, match perfectly with the strong emissions at 450 and 475 nm and weak emission at 635 nm from PEO-UCs (Figure 4a). The ZnTPTBP was successfully bottom-up-prepared (see Scheme S1 in the ESI) by firstly synthesizing 5,10,15,20-tetraphenyltetraabenzoporphyrins ($\text{H}_2\text{-8H-TPTBP}$) (see Figure S3 for MS of $\text{H}_2\text{-8H-TPTBP}$ in the ESI). The $\text{H}_2\text{-8H-TPTBP}$ was used as starting material to synthesize 5,10,15,20-tetraphenyltetraabenzoporphyrins (H_2TPTBP) (see Figure S4 and S5 for ^1H NMR and MS of H_2TPTBP in the ESI). After that, the zinc metallation of H_2TPTBP was carried out to yield ZnTPTBP, which was purified to 95% purity through column chromatography (see Figure S6 and S7 in the ESI for ^1H NMR and MS of ZnTPTBP).

Loading of ZnTPTBP onto PEO-UCs

ZnTPTBP molecules were loaded onto the PEO-UCs by incubating them together in water. The obtained green particles of ZnTPTBP-loaded PEO-UCs or the so-called ZnTPTBP-UCs were collected by centrifugation. It should be noted here that when only water or the

COOH-PEO-COOH ligand was used in place of PEO-UCs, no solid was observed after centrifugation. This implied that without the PEO-UCs, the ZnTPTBP would not precipitate out under the condition used. To further make sure that the obtained solid from the centrifugation contained no ZnTPTBP precipitate, the product was resuspended in water and scanned for precipitate under microscope. No precipitate was observed. Noted that both the ICP-OES analysis of the centrifuged crystals and also the indirect quantitation of unabsorbed dyes in the supernatant obtained during the isolation of ZnTPTBP-UCs from the mixture, gave agreeable ZnTPTBP loading content of $\sim 2 - 3\%$ (2.3% and 3.0% for the former and the latter analysis methods, respectively). The efficiency of the loading process was $\sim 77 - 100\%$. This excellent loading efficiency correlated well with the small amount of ZnTPTBP used in the loading process and also the water insolubility of the dye molecules.

At the same NIR illumination and the same PEO-UCs concentration, fluorescence spectra of PEO-UCs showed higher emission intensities at 450, 475 and 635 nm than those of the ZnTPTBP-UCs (Figure 4a). The decrease of the emission upon the ZnTPTBP loading was most pronounced at the 450 and 470 nm, and this corresponded well with the intense B-band absorption at 430-490 nm of the ZnTPTBP. The decrease at 635 nm was less pronounced and this agreed with the small Q-band absorption at 635 nm of ZnTPTBP. The small decrease was also observed for the 360 and 365 nm emissions, and this was probably due to a small absorption tail around the UVA region of the ZnTPTBP. The result suggested that radiations emitted from the UCs upon 980 nm excitation, could be efficiently absorbed by the loaded ZnTPTBP. This process makes it possible for the ZnTPTBP-UCs to act as photosensitizer with NIR excitation. We, therefore, proof for an ability of ZnTPTBP-UCs to generate excited singlet oxygen species [$\text{O}_2(^1\Delta_g)$] under NIR irradiation.

Production of singlet oxygen

To demonstrate the production of singlet oxygen, the aqueous suspension of ZnTPTBP-UCs was irradiated with 980 nm laser in a presence of 9,10-anthracenediyl-bis(methylene)dimalonic acid (ABDA), a singlet oxygen probe.³³ Singlet oxygen can oxidize ABDA into an endoperoxide form, which leads to a decrease of its fluorescence intensity at 430 nm. Therefore, the presence of the singlet oxygen in the system can be detected through the decrease of the ABDA fluorescence emission at 430 nm (when excited at 380 nm). Here we monitored the level of ABDA fluorescence with increasing time of 980 nm irradiation for the PEO-UCs, ZnTPTBP and ZnTPTBP-UCs samples. The decrease was most prominent for ZnTPTBP-UCs, followed with the PEO-UCs, whereas the ZnTPTBP produced no decrease (Figure 4b). To confirm that the decrease of ABDA fluorescence was surely from singlet oxygen, sodium azide (NaN_3), a singlet oxygen scavenger, was used. As predicted, significantly less decrease in the 430 nm emissions was observed in the presence of NaN_3 for both the ZnTPTBP-UCs and the PEO-UCs (Figure 4b). This, therefore, confirmed the generation of singlet oxygen species of the PEO-UCs and the ZnTPTBP-UCs upon NIR

irradiation. As expected, the ZnTPTBP alone could not produce singlet oxygen upon the NIR irradiation (Figure 4b). The ability of the ZnTPTBP-UCs to effectively produce singlet oxygen species agrees well with our design for the absorption of the upconverted photons by the loaded dyes. The singlet oxygen production and the decrease in emission intensity upon dye loading verify the absorption of the UC's emission by the loaded dye molecules.

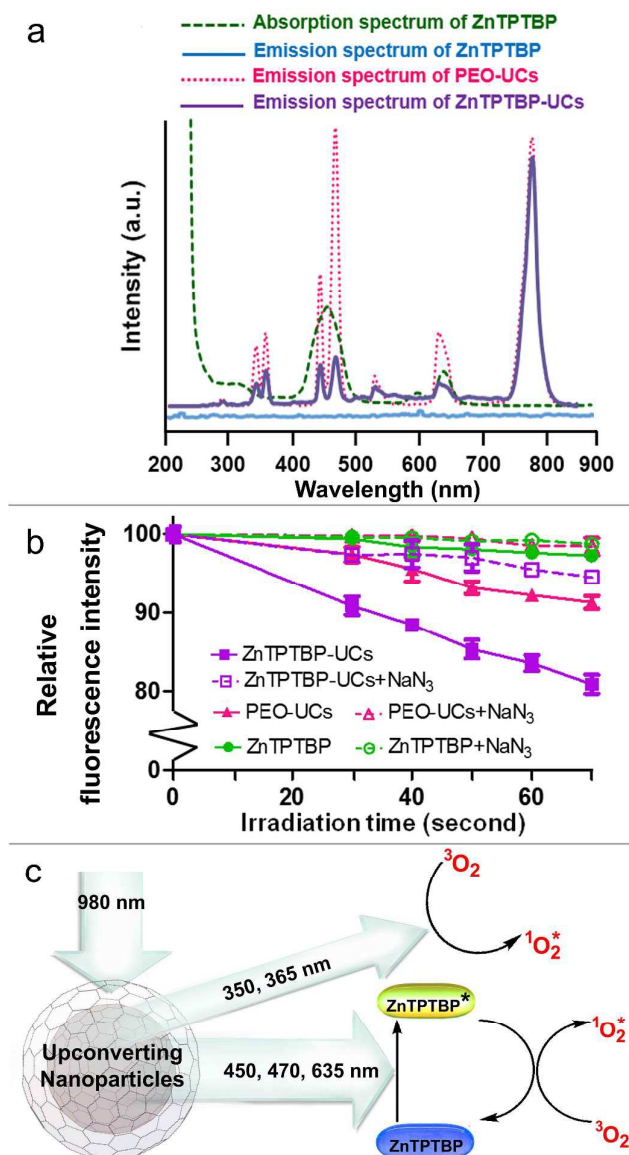


Figure 4. Harmony between emissions from UCs and absorptions of photosensitizer: a) Absorption spectrum of 34 μM ZnTPTBP, and emission spectra of PEO-UCs (1000 $\mu\text{g}/\text{mL}$), ZnTPTBP (34 μM) and ZnTPTBP-UCs (34 μM ZnTPTBP and 1000 $\mu\text{g}/\text{mL}$ PEO-UCs) (λ_{ex} of 980 nm); b) Fluorescence intensity of the singlet oxygen probe ABDA mixed with PEO-UCs, ZnTPTBP, ZnTPTBP-UCs, PEO-UCs + NaN₃, ZnTPTBP + NaN₃ and ZnTPTBP-UCs + NaN₃ under various times of 980 nm irradiation ($\lambda_{\text{em}}/\lambda_{\text{ex}}$ of 430/380 nm), data shown as mean \pm SD ($n=6$) from two independent experiments, ZnTPTBP and PEO-

UCs concentrations of 17 μM and 500 $\mu\text{g}/\text{mL}$, respectively; c) Model showing the production of singlet oxygen by ZnTPTBP-UCs under 980 nm irradiation.

These results indicate that the PEO-UCs can generate singlet oxygen upon 980 nm irradiation. This agrees well to the ability of the PEO-UCs to upconvert NIR into UVA. Noted here that UVA radiation can activate the ground state triplet oxygen into excited singlet oxygen.³⁴ We explained the more efficient singlet oxygen production of the ZnTPTBP-UCs over the PEO-UCs as followed: in addition to the generation of singlet oxygen by the UVA emission from the PEO-UCs, here the visible radiations (450, 470 and 635 nm) emitted from the PEO-UCs upon NIR excitation were absorbed by the loaded ZnTPTBP, the excited ZnTPTBP molecules then sensitized ground state oxygen molecules, producing excited singlet oxygen species (Figure 4c).

In vitro cytotoxicity

We investigated the biocompatibility of PEO-UCs, ZnTPTBP and ZnTPTBP-UCs, using the A-375 cell line by incubating the tested particles with the cells for 24 h and determining cell viability using MTT assay. Both particles showed no significant effect on viability of the A-375 cells when used at the concentrations of up to 500 $\mu\text{g}/\text{mL}$ under no NIR irradiation, i.e., more than 80% cell survival was observed (Figure S8 in ESI). Upon the NIR exposure at 560 J/cm^2 , cytotoxicity of the PEO-UCs at 500 $\mu\text{g}/\text{mL}$ increased to approximately 30 % cell death (shown in Figure S8 as 70 % cell survival). The result corresponds well with an ability of the PEO-UCs to produce some singlet oxygen species upon NIR irradiation (Figure 4b). The cytotoxicity was more pronounced for the ZnTPTBP-UCs; at the same NIR exposure and the same PEO-UCs concentration of 500 $\mu\text{g}/\text{mL}$, ~ 50 % cell survival was observed. The better ability of the ZnTPTBP-UCs to produce reactive oxygen, as compared to that of the unloaded PEO-UCs, is likely responsible for its higher cytotoxicity under NIR irradiation. Next we investigated an ability of the material to inhibit the growth and kill *P. acnes*.

Anti-*P. acnes* photodynamic action

Based on the evidences that the singlet oxygen could help eradicating *P. acnes*,²¹ and photo-excitation of the bacterial porphyrins could also kill the bacteria,²⁰⁻²² therefore, the ZnTPTBP-UCs combined with NIR light should be an effective tools for *P. acnes* eradication. With the effective singlet oxygen production upon NIR irradiation, the UVA emissions that match with the absorption ranges of *P. acnes* porphyrins, and water dispersible character of the ZnTPTBP-UCs, we propose to use the NIR assisted ZnTPTBP-UCs for acne treatment. Therefore, here we show the in vitro anti-*P. acnes* activity of the material under NIR irradiation.

Growth of *P. acnes* after irradiation with a 980 nm laser was first studied. The experiments were carried out using a bacterial broth method and the viable bacteria were quantified with *p*-iodonitrotetrazolium violet (INT). We observed that the *P. acnes* viability was not affected by 480 J/cm^2 of NIR irradiation (Table 1). The same result was observed when ZnTPTBP was added. These results suggest that either in the presence or in the absence of the

photosensitizer ZnTPTBP, the *P. acnes* are not sensitive to 980 nm at the exposure of 480 J/cm². However, in the presence of either the PEO-UCs or the ZnTPTBP-UCs, growth inhibition of the *P. acnes* was observed under the 480 J/cm² NIR irradiation (Table 1). The ZnTPTBP-UCs were more effective than the PEO-UCs in inhibiting the growth of *P. acnes*, i.e., less NIR radiation was needed to inhibit the bacterial growth in the presence of the ZnTPTBP-UCs as compared to that in the presence of unloaded PEO-UCs. The results conform well to our hypothesis that upon the NIR irradiation, PEO-UCs emit UVA that harms the *P. acnes* by the photo-excitation of oxygen into reactive oxygen species (ROS)³⁴ and the photo-excitation of porphyrins in the bacteria. As shown above that at similar NIR exposure, ZnTPTBP-UCs could produce singlet oxygen more effectively than the unloaded PEO-UCs (Figure 4b), it was not surprised to observe here that at similar NIR exposure, the former could inhibit the *P. acnes* growth more efficiently than the latter.

Table 1. *P. acnes* growth in the presence of PEO-UCs, ZnTPTBP and ZnTPTBP-UCs at various exposures of the 980 nm laser.

Samples	Exposures (J/cm ²)				
	0	240	320	400	480
Water	-	-	-	-	-
ZnTPTBP (15 µg/mL)	-	-	-	-	-
PEO-UCs (500 µg/mL)	-	-	-	-	+
ZnTPTBP-UCs (15 µg/mL ZnTPTBP, 500 µg/mL PEO-UCs)	-	-	-	+	+

The result indicates that the ZnTPTBP-UCs and the PEO-UCs can be used in conjunction with the 980 nm laser for the *P. acnes* combat. We, therefore, investigated the MIC and the MBC values of these two materials against *P. acnes* under NIR irradiation. Here we fixed the 980 nm irradiance at 560 J/cm², and varied the concentrations of tested samples by two-fold serial dilution. As expected, ZnTPTBP-UCs gave lower MIC and lower MBC values than the unloaded PEO-UCs (Table 2). It should be noted here that at the MBC of the ZnTPTBP-UCs under NIR exposure, the cytotoxicity against A-375 was at 50 % cell survival (Figure S8 in ESI). Therefore, we observed here the ability of the ZnTPTBP-UCs to completely killed *P. acnes* under the condition that 50 % A-375 cells could still survive (Figure S8 in ESI). Interestingly, although the MBC concentration of unloaded PEO-UCs was double of that of the ZnTPTBP-loaded UCs, this PEO-UCs concentration caused only 30 % death of the A-375 cells under NIR radiation (Figure S8 in ESI). The reason for this is likely that without ZnTPTBP loading, the direct photo-excitation of porphyrin in the bacteria by the UVA emitted from the PEO-UCs probably predominated over the reactive oxygen species production. In contrast, with the ZnTPTBP being loaded on the PEO-UCs, high amount of singlet oxygen was generated and these excited oxygen species could harm both the bacteria and other cells. Further study on the fine tuning of the laser power, the duration of the laser, the amounts of both the PEO-UCs and ZnTPTBP will be needed in vivo to obtain the maximal bacterial harm with minimal damage to skin cells.

Table 2. The photoinactivation of *P. acnes* tested at 980 nm, radiation of 560 J/cm²

Sample	MIC (µg/mL)	MBC (µg/mL)
PEO-UCs	500	1000
ZnTPTBP-UCs	PEO-UCs = 250 ZnTPTBP = 7.5	PEO-UCs = 500 ZnTPTBP = 15

Conclusions

In conclusion, we have successfully demonstrated the NIR assisted photosensitizer-loaded upconverting nanoparticles that can eradicate *P. acne*. The synthesis of a water dispersible, non-toxic, hexagonal phase core/shell upconverting nanoparticles with high UVA and visible emissions is shown through the optimization of the doping amount of Yb³⁺, Tm³⁺ in the NaYF₄ core lattice and constructing the NaYF₄ shell around the core UCs. The obtained UCs, which is the (0.2 mol% Tm³⁺, 30 mol% Yb³⁺)-doped NaYF₄/NaYF₄ core/shell nanoparticles, can destroy *P. acnes* in vitro under NIR irradiation. To improve the anti-*P. acnes* photodynamic therapy, the synthesis of the ZnTPTBP photosensitizer whose absorption wavelengths perfectly match with the visible emission wavelengths of the obtained UCs, is demonstrated. The obtained photosensitizer-loaded UCs can effectively produce singlet oxygen under NIR irradiation. In vitro *P. acnes* eradication using the combination of 980 nm laser and the obtained photosensitizer-loaded UCs requires less NIR laser than that using unloaded UCs. The MIC and MBC values of the materials are reported. This work thus paves the way for a new photodynamic therapy of *P. acnes* using the combination of bio-transparent NIR light and the photosensitizer-loaded UCs. This work also shows that a perfect harmony between the emissions of UCs and the absorptions of photosensitizer, can make photodynamic therapy with NIR laser effective.

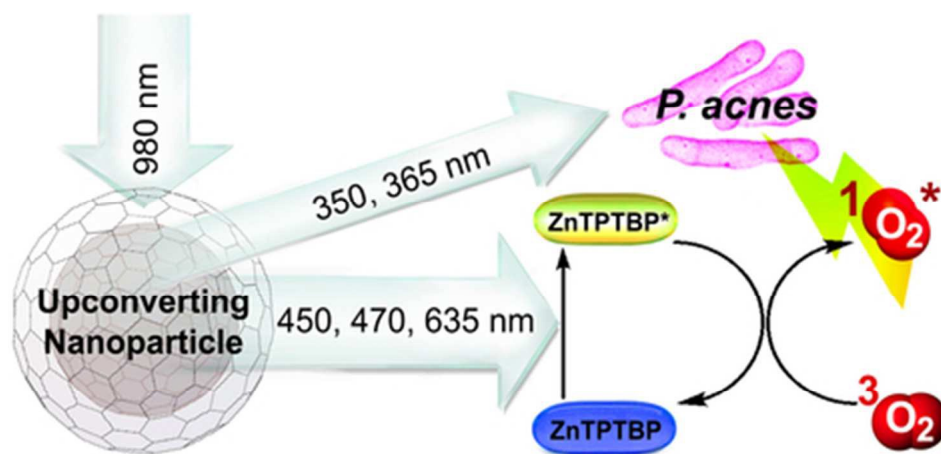
Acknowledgements

This work was financially supported by the Ratchadapiseksompot Fund (GCRS58032301) from Chulalongkorn University (CU), Food and Water Cluster (WCU-58-011-FW) from CU, Nanotec-CU Center of Excellence on Food and Agriculture, Thailand. T. T.-U. is funded by the Development and Promotion of Science and Technology talents project (Thailand). The inductively coupled plasma optical emission spectrometer was provided courtesy of Sci Spec Co., Ltd. (Thermo Scientific, iCAP 6500).

Notes and references

- 1 Y. N. Konan, R. Gurny and E. Allémann, *Journal of Photochemistry and Photobiology B: Biology*, 2002, **66**, 89-106.
- 2 M. Fernández-Guarino, I. García-Morales, A. Harto, C. Montull, B. Pérez-García and P. Jaén, *Actas Dermo-Sifiliográficas (English Edition)*, 2007, **98**, 377-395.
- 3 F. Wang and X. Liu, *Chemical Society Reviews*, 2009, **38**, 976-989.

- 4 D. K. Chatterjee, A. J. Rufaihah and Y. Zhang, *Biomaterials*, 2008, **29**, 937-943.
- 5 M. Nyk, R. Kumar, T. Y. Ohulchanskyy, E. J. Bergey and P. N. Prasad, *Nano Letters*, 2008, **8**, 3834-3838.
- 6 L. Zhou, B. He, J. Huang, Z. Cheng, X. Xu and C. Wei, *ACS Applied Materials & Interfaces*, 2014, **6**, 7719-7727.
- 7 M. Yu, F. Li, Z. Chen, H. Hu, C. Zhan, H. Yang and C. Huang, *Analytical Chemistry*, 2009, **81**, 930-935.
- 8 L. Cheng, K. Yang, S. Zhang, M. Shao, S. Lee and Z. Liu, *Nano Res.*, 2010, **3**, 722-732.
- 9 Q. Liu, Y. Sun, C. Li, J. Zhou, C. Li, T. Yang, X. Zhang, T. Yi, D. Wu and F. Li, *ACS Nano*, 2011, **5**, 3146-3157.
- 10 X. Niu, H. Chen, Y. Wang, W. Wang, X. Sun and L. Chen, *ACS Applied Materials & Interfaces*, 2014, **6**, 5152-5160.
- 11 L. He, L. Feng, L. Cheng, Y. Liu, Z. Li, R. Peng, Y. Li, L. Guo and Z. Liu, *ACS Applied Materials & Interfaces*, 2013, **5**, 10381-10388.
- 12 M. K. G. Jayakumar, N. M. Idris and Y. Zhang, *Proceedings of the National Academy of Sciences*, 2012, **109**, 8483-8488.
- 13 S. Gai, P. Yang, C. Li, W. Wang, Y. Dai, N. Niu and J. Lin, *Advanced Functional Materials*, 2010, **20**, 1166-1172.
- 14 L. L. Fedoryshin, A. J. Tavares, E. Petryayeva, S. Doughan and U. J. Krull, *ACS Applied Materials & Interfaces*, 2014, **6**, 13600-13606.
- 15 D. K. Chatterjee and Z. Yong, *Nanomedicine*, 2008, **3**, 73-82.
- 16 C. Wang, H. Tao, L. Cheng and Z. Liu, *Biomaterials*, 2011, **32**, 6145-6154.
- 17 N. M. Idris, M. K. Gnanasammandhan, J. Zhang, P. C. Ho, R. Mahendran and Y. Zhang, *Nature Medicine*, 2012, **18**, 1580-1585.
- 18 S. Cui, D. Yin, Y. Chen, Y. Di, H. Chen, Y. Ma, S. Achilefu and Y. Gu, *ACS Nano*, 2013, **7**, 676-688.
- 19 H. Wang, Z. Liu, S. Wang, C. Dong, X. Gong, P. Zhao and J. Chang, *ACS Applied Materials & Interfaces*, 2014, **6**, 3219-3225.
- 20 T. B. Melø, *Zeitschrift für Naturforschung. C, Journal of biosciences*, 1987, **42**, 123-128.
- 21 K. Arakane, A. Ryu, C. Hayashi, T. Masunaga, K. Shinmoto, S. Mashiko, T. Nagano and M. Hirobe, *Biochemical and Biophysical Research Communications*, 1996, **223**, 578-582.
- 22 H. Ashkenazi, Z. Malik, Y. Harth and Y. Nitzan, *FEMS Immunology and Medical Microbiology*, 2003, **35**, 17-24.
- 23 M. A. Filatov, A. V. Cheprakov and I. P. Beletskaya, *European Journal of Organic Chemistry*, 2007, 3468-3475.
- 24 J. Jiao, P. Thammyongkit, I. Schmidt, J. S. Lindsey and D. F. Bocian, *The Journal of Physical Chemistry C*, 2007, **111**, 12693-12704.
- 25 J. C. Boyer, C. J. Carling, B. D. Gates and N. R. Branda, *Journal of the American Chemical Society*, 2010, **132**, 15766-15772.
- 26 G. Jiang, J. Pichaandi, N. J. J. Johnson, R. D. Burke and F. C. J. M. van Veggel, *Langmuir*, 2012, **28**, 3239-3247.
- 27 A. Yin, Y. Zhang, L. Sun and C. Yan, *Nanoscale*, 2010, **2**, 953-959.
- 28 G. S. Yi and G. M. Chow, *Chemistry of Materials*, 2007, **19**, 341-343.
- 29 L. B. Josefsen and R. W. Boyle, *Theranostics*, 2012, **2**, 916-966.
- 30 M. Ethirajan, Y. Chen, P. Joshi and R. K. Pandey, *Chemical Society Reviews*, 2011, **40**, 340-362.
- 31 C. M. B. Carvalho, T. J. Brocksom and K. T. de Oliveira, *Chemical Society Reviews*, 2013, **42**, 3302-3317.
- 32 A. Y. Lebedev, M. A. Filatov, A. V. Cheprakov and S. A. Vinogradov, *The Journal of Physical Chemistry A*, 2008, **112**, 7723-7733.
- 33 N. A. Kuznetsova, N. S. Gretsova, O. A. Yuzhakova, V. M. Negrinovskii, O. L. Kaliya and E. A. Luk'yanets, *Russian Journal of General Chemistry*, 2001, **71**, 36-41.
- 34 R. M. Tyrrell, in *Methods in Enzymology*, ed. H. S. Lester Packer, Academic Press, 2000, Volume 319, pp. 290-296.



Graphical abstract
39x19mm (300 x 300 DPI)